

Impact of Top SiO₂ Interlayer Thickness on Memory Window of Si Channel FeFET with TiN/SiO₂/Hf_{0.5}Zr_{0.5}O₂/SiO_x/Si (MIFIS) Gate Structure

Tao Hu, Xianzhou Shao, Mingkai Bai, Xinpei Jia, Saifei Dai, Xiaoqing Sun, Runhao Han, Jia Yang, Xiaoyu Ke, Fengbin Tian, Shuai Yang, Junshuai Chai, Hao Xu, Xiaolei Wang, Wenwu Wang, and Tianchun Ye

Abstract—We study the impact of top SiO₂ interlayer thickness on the memory window (MW) of Si channel ferroelectric field-effect transistor (FeFET) with TiN/SiO₂/Hf_{0.5}Zr_{0.5}O₂/SiO_x/Si (MIFIS) gate structure. We find that the MW increases with the increasing thickness of the top SiO₂ interlayer, and such an increase exhibits a two-stage linear dependence. The physical origin is the presence of the different interfacial charges trapped at the top SiO₂/Hf_{0.5}Zr_{0.5}O₂ interface. Moreover, we investigate the dependence of endurance characteristics on initial MW. We find that the endurance characteristic degrades with increasing the initial MW. By inserting a 3.4 nm SiO₂ dielectric interlayer between the gate metal TiN and the ferroelectric Hf_{0.5}Zr_{0.5}O₂, we achieve a MW of 6.3 V and retention over 10 years. Our work is helpful in the device design of FeFET.

Index Terms—FeFET, memory window, Hf_{0.5}Zr_{0.5}O₂, MIFIS gate structure, charge trapping.

I. INTRODUCTION

Hafnia(HfO₂) based silicon channel ferroelectric field-effect transistors (HfO₂ Si-FeFETs) have been extensively studied, as a strong candidate for non-volatile memory with lower power operation, fast speed, and CMOS compatibility [1-13], thanks to the discovery of ferroelectricity in doped-HfO₂ [14]. The large spontaneous polarization (P_s) of ferroelectric doped-HfO₂ ($\sim 2\text{-}30 \mu\text{C}/\text{cm}^2$) induces significant charge trapping and de-trapping phenomenon, and this results in the decrease of the memory window (MW) [15-18]. To suppress the charge trapping and de-trapping effect, several studies focus on suppressing the charge injection from the silicon channel to the ferroelectric Hf_{0.5}Zr_{0.5}O₂/Si interface, such as applying high- κ interlayer [19-23], reducing the spontaneous polarization of ferroelectric [24-27], and eliminating interlayer [28-32]. However, the above method cannot significantly improve the MW and the MW is generally limited to less than

2 V. This MW does not meet the requirements for application in multi-bit memory cells. Recently, inserting a dielectric layer (e.g. SiO₂ or Al₂O₃) between the metal gate and ferroelectric layer was found to be an effective method to significantly improve the MW [33-38]. The MW can achieve 3.8 V by inserting 2 nm SiO₂ and 4.1 V by inserting 3 nm Al₂O₃ [34, 38]. Moreover, the simulation results show that using a low dielectric constant and thick interlayer (such as SiO₂) is beneficial for the MW increase [35].

However, there are still no experimental studies on this issue and the impact of the top SiO₂ interlayer thickness on the MW is still unclear. Therefore, we experimentally report the dependence of the MW on the top SiO₂ interlayer thickness in this work and discuss its physical origin. The physical origin of the impact of the top SiO₂ thickness on the MW is attributed to two discrete defect energy levels. We find that the MW increases with the increasing thickness of the top SiO₂ interlayer. We achieve a maximum MW of 6.3 V by inserting a 3.4 nm top SiO₂ interlayer. Furthermore, we study the dependence of the endurance characteristics on initial MW. We find that the endurance characteristic degrades with increasing the initial MW. We realize an endurance of $\sim 10^4$ cycles with an initial MW of 5.3 V by inserting a 3.4 nm top SiO₂ interlayer.

II. DEVICE FABRICATION AND CHARACTERIZATION

Fig. 1 shows the schematic of the device structure and fabrication process flow. In this work, there are two different gate stacks. One is TiN/Hf_{0.5}Zr_{0.5}O₂/SiO_x/Si (MFIS) as the control sample. The other is TiN/SiO₂/Hf_{0.5}Zr_{0.5}O₂/SiO_x/Si (MIFIS) with a 0.85, 1.7, 2.55, or 3.4 nm top SiO₂ interlayer.

These devices were fabricated in an 8-inch P-type silicon wafer with a resistivity of 8-12 $\Omega\cdot\text{cm}$ using a gate-last process. Firstly, B ions with an energy of 60 KeV and a dose of $8 \times 10^{12} \text{ cm}^{-2}$ were implanted into the whole Si substrate. After that, the Si substrate was annealed at 1050 °C for 4 h and 1150 °C for 40 min to form a P-type well. Next, the source and drain regions

This work was supported by the National Natural Science Foundation of China under Grant No. 92264104 and 52350195 and the Postdoctoral Fellowship Program of CPSF under Grant No. GZC20232925. (Corresponding author: Xiaolei Wang)

Tao Hu, Xianzhou Shao, Mingkai Bai, Xinpei Jia, Saifei Dai, Xiaoqing Sun, Runhao Han, Jia Yang, Xiaoyu Ke, Fengbin Tian, Shuai Yang,

Junshuai Chai, Hao Xu, Xiaolei Wang, Wenwu Wang, and Tianchun Ye are with Institute of microelectronics of the Chinese Academy of Sciences, Beijing 100029, China. The authors are also with the School of Integrated Circuits, University of Chinese Academy of Sciences, Beijing 100049, China (e-mail: wangxiaolei@ime.ac.cn).

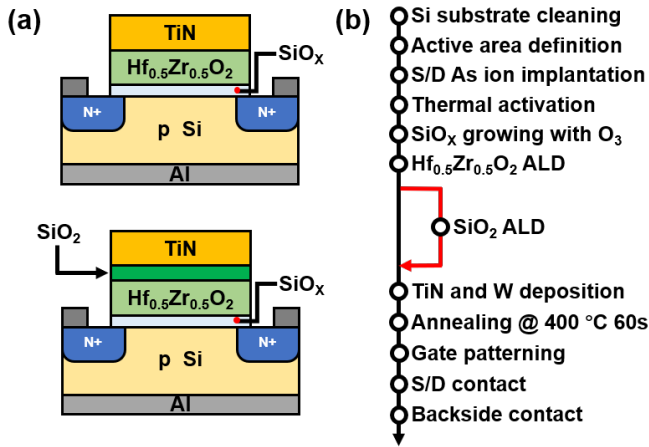


Fig. 1. (a) Schematic of the HfO₂ Si-FeFET device structure and (b) fabrication process flow.

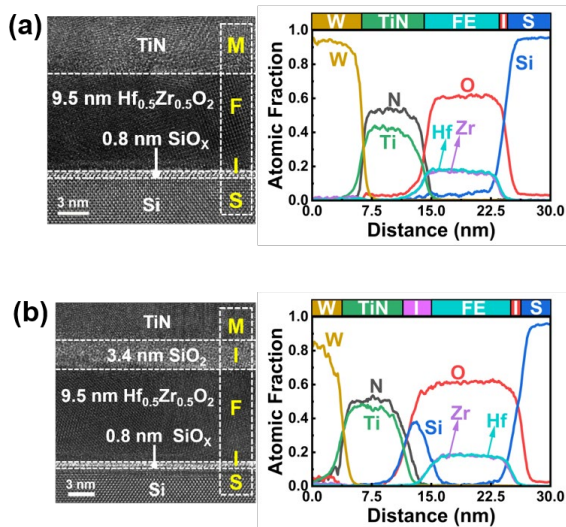


Fig. 2. HRTEM images and EDS of the (a) MFIS and (b) MIFIS structures.

were defined through photolithography. Then As ions with an energy of 50 KeV and a dose of $2 \times 10^{15} \text{ cm}^{-2}$ were implanted into source and drain regions. After that, these devices were annealed at 1050 °C for 5 s under the N₂ atmosphere for dopant activation. Subsequently, the gate stack was formed. After diluted-HF clean, the 0.8 nm bottom SiO_x interlayer was grown by ozone oxidation at 300 °C. Then, 9.5 nm Hf_{0.5}Zr_{0.5}O₂ and 0.85-3.4 nm top SiO₂ interlayer were grown by atomic layer deposition (ALD) at 300 °C. For the growth of ALD Hf_{0.5}Zr_{0.5}O₂, the tetrakis-(ethylmethylamino)-hafnium (TEMA-Hf), tetrakis-(ethylmethylamino)-zirconium (TEMA-Zr), and H₂O were used as precursors of Hf, Zr, and O, respectively. For the growth of ALD SiO₂, the bis(diethylamino)silane (BDEAS) and ozone were used as precursors of Si and O, respectively. Then, 10 nm TiN was grown by physical vapor deposition (PVD) and 75 nm W was grown by ALD. The devices were annealed at 400 °C under an N₂ atmosphere for 60 s by using rapid thermal annealing (RTA) to form the orthorhombic phase. Finally, the forming gas annealing (FGA) was performed at 450 °C in 5%-H₂/95%-N₂ to passivate the defects of the gate stack. All of the fabrication processes of the MFIS structure were the same as the MIFIS structure, except without the top

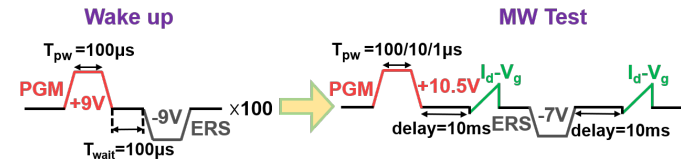


Fig. 3. Waveforms of electrical measurement.

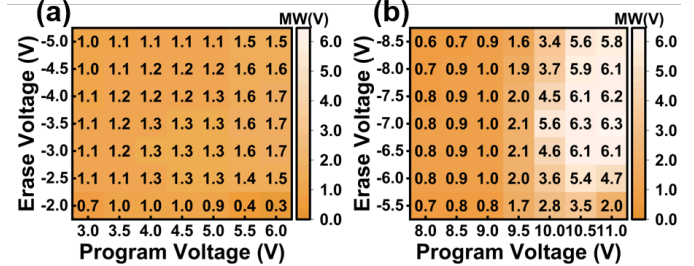


Fig. 4. The MW mapping of (a) MFIS and (b) MIFIS with 3.4 nm top SiO₂ as a function of the pulse amplitude under the pulse width of 100 μs.

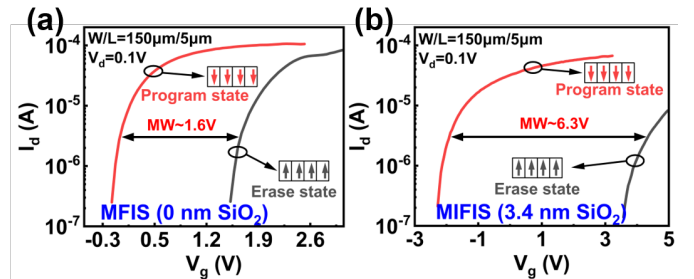


Fig. 5. I_d-V_g curves of the maximum MW for (a) MFIS and (b) MIFIS with 3.4 nm top SiO₂ interlayer under the pulse width of 100 μs.

dielectric interlayer SiO₂.

Fig. 2 shows High-Resolution Transmission Electron Microscopy (HRTEM) images and Energy Dispersion Spectrometer (EDS) results for both MFIS and MIFIS structures. For the MIFIS structure, the presence of a peak concentration of Si at the TiN/Hf_{0.5}Zr_{0.5}O₂ interface confirms the presence of the top SiO₂ interlayer.

In this work, the gate length/width (L/W) of these devices is 5/150 μm. The electrical measures were performed by Keysight B1500A with a waveform generator fast measurement unit (WGFMU) and high voltage semiconductor pulse generator unit (SPGU). The threshold voltage (V_{th}) is extracted by the constant current method at the drain current I_d = W/L × 10⁻⁷ A.

III. RESULTS AND DISCUSSIONS

A. The dependence of MW on the top SiO₂ thickness

We investigate the dependence of the MW on the pulse amplitude. Fig. 3 shows the MW measurement waveforms. The pulse width is set as 100 μs. Fig. 4 shows the MW mapping results for the MFIS and MIFIS structure with the 3.4 nm top SiO₂ interlayer (unless specified otherwise in the following context, MIFIS structure refers to the MIFIS structure with the 3.4 nm top SiO₂ interlayer). For the MFIS or MIFIS structure, when the program pulse amplitude goes beyond 6 V or 11 V under the pulse width of 100 μs, respectively, the devices break down. Thus, we find that the maximum MW is 6.3 V for the

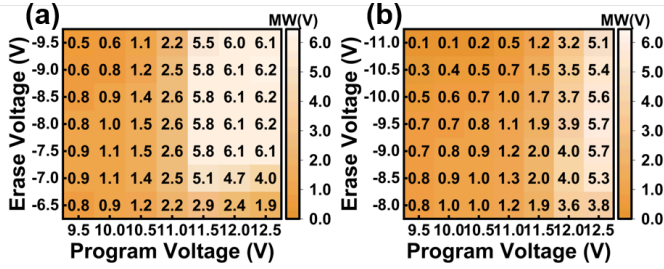


Fig. 6. The MW mapping of MIFIS with 3.4 nm top SiO₂ as a function of the pulse amplitude under the pulse width of (a) 10 μs and (b) 1 μs.

MIFIS structure with the 3.4 nm top SiO₂ interlayer, while the maximum MW is 1.7 V for the MFIS sample. Fig. 5(a) and (b) show the I_t - V_g curves corresponding to the maximum MW for the MFIS and MIFIS structures, respectively.

We repeated the above measurement process under the different pulse widths. Fig. 6(a) and (b) show the MW mapping results for the MIFIS structure under the pulse width of 10 μs and 1 μs. The results are similar to the pulse width of 100 μs in Fig. 4. Thus the pulse width does not affect the conclusion in this work.

We investigate the impact of top SiO₂ interlayer thickness on the maximum MW. For each sample, we repeated the above MW mapping measurement process. Fig. 7(a) shows the dependence of the maximum MW on the top SiO₂ interlayer thickness. Fig. 7(b) shows the dependence of the V_{th} on the top SiO₂ interlayer thickness corresponding to the maximum MW in Fig. 7(a). From Fig. 7, we can see that the maximum MW of the MIFIS structure increases with top SiO₂ thickness. Moreover, the curve of the maximum MW vs. the top SiO₂ thickness exhibits a two-stage linear relationship.

B. The physical origin of the MW dependence on the top SiO₂ thickness

Firstly, we discuss the physical origin of MW enlargement by inserting the top SiO₂ interlayer compared with the sample without the top SiO₂ interlayer. The origin is charge trapping between the TiN metal gate and the top SiO₂/Hf_{0.5}Zr_{0.5}O₂ interface [34, 35, 38]. During the erase pulse, electrons trapping and/or holes de-trapping at the top SiO₂/Hf_{0.5}Zr_{0.5}O₂ interface occurs. This results in negative charges at the top SiO₂/Hf_{0.5}Zr_{0.5}O₂ interface because the top SiO₂ acts as a barrier layer after the erase operation. Then the V_{th} positively shifts. During the program pulse, electrons de-trapping and/or holes trapping at the top SiO₂/Hf_{0.5}Zr_{0.5}O₂ interface occurs. This results in positive charges at the top SiO₂/Hf_{0.5}Zr_{0.5}O₂ interface after the program. Then the V_{th} negatively shifts. Finally, the above results lead to a large MW. Fig. 7(b) supports the above discussion.

Secondly, we discuss the physical origin of the dependence of the maximum MW on the top SiO₂ thickness. Due to the presence of the trapped charges (Q_{tp}) at the top SiO₂/Hf_{0.5}Zr_{0.5}O₂ interface, the shift of the threshold voltage (ΔV_{th}) with respect to the control sample is calculated by

$$\Delta V_{th} = - \frac{Q_{tp}}{\epsilon_0 \epsilon_{SiO_2}} \cdot d_{SiO_2} \quad (1)$$

where ϵ_0 is the vacuum dielectric constant, ϵ_{SiO_2} is the relative

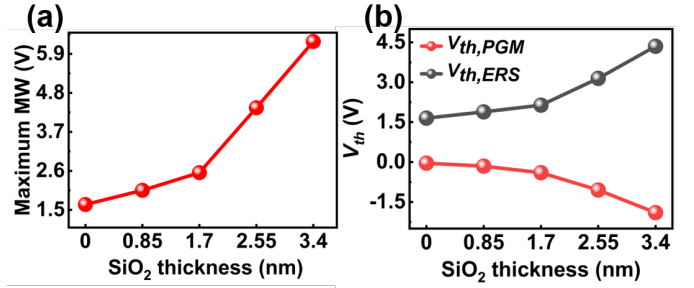


Fig. 7. The dependence of (a) the maximum MW and (b) the V_{th} corresponding to the maximum MW on the top SiO₂ interlayer thickness.

dielectric constant of the top SiO₂ interlayer, and d_{SiO_2} is the physical thickness of the top SiO₂ interlayer. When the interfacial charges (Q_{tp}) remain constant, the shift of the threshold voltage (ΔV_{th}) is linearly dependent on the top SiO₂ thickness. Thus, the results indicate that the two-stage relationship between the maximum MW and the top SiO₂ thickness as shown in Fig. 7(a) is due to the presence of different interfacial charges Q_{tp} , which increases with an increase in the thickness of the top SiO₂.

We use the energy band diagram to discuss the physical origin. Fig. 8(a) shows the band diagram of the MIFIS during the erase operation. We consider that both donor and acceptor traps appear at the top SiO₂/Hf_{0.5}Zr_{0.5}O₂ interface. The donor and acceptor traps are located near the valence and conduction band of Hf_{0.5}Zr_{0.5}O₂, respectively. During the erase operation, the electric field across the top SiO₂ interlayer is nearly close to its breakdown field due to the large spontaneous polarization P_s (~20 μC/cm²) of the ferroelectric Hf_{0.5}Zr_{0.5}O₂. This results in significant band bending of the top SiO₂ interlayer. Thus, the Fermi energy level of the gate metal TiN with the thicker top SiO₂ interlayer is higher than that of the thinner top SiO₂ interlayer. Then the donor traps are filled by the tunneling electrons regardless of the top SiO₂ thickness and show neutral charges. For the SiO₂ thickness of less than 1.7 nm, the Fermi energy level of the gate metal TiN is always located above the acceptor trap energy level $E_{a,1}$ during the erase operation. The acceptor trap energy level $E_{a,1}$ is also filled by the electrons and shows negative charges. After the erase operation, these negative charges are left as shown in Fig. 8(b), and lead to the positive shift of V_{th} after the erase operation ($V_{th,ERS}$) as shown in Fig. 7(b). Moreover, for the SiO₂ thickness of less than 1.7 nm, these negative charges determined by acceptor trap energy level $E_{a,1}$ after the erase operation are nearly identical, and this results in the first stage of $V_{th,ERS}$ vs. the top SiO₂ thickness curve as shown in Fig. 7(b).

We discuss the physical origin of the second stage of the erase case. The second stage indicates that the acceptor traps have two levels, which is schematically shown in Fig. 8(a). For the SiO₂ thickness of less than 1.7 nm, the acceptor trap energy level $E_{a,1}$ is filled by the electrons and the acceptor trap energy level $E_{a,2}$ is empty. For thicker SiO₂ thickness of larger than 1.7 nm, however, both the acceptor trap energy level $E_{a,2}$ and $E_{a,1}$ are filled because thicker SiO₂ induces a larger voltage drop across the whole top SiO₂ interlayer and higher Fermi level of the metal gate with respect to the trap levels as shown in Fig. 8(a). Then more negative charges are trapped for thicker SiO₂ thickness of larger than 1.7 nm, and result in the second stage

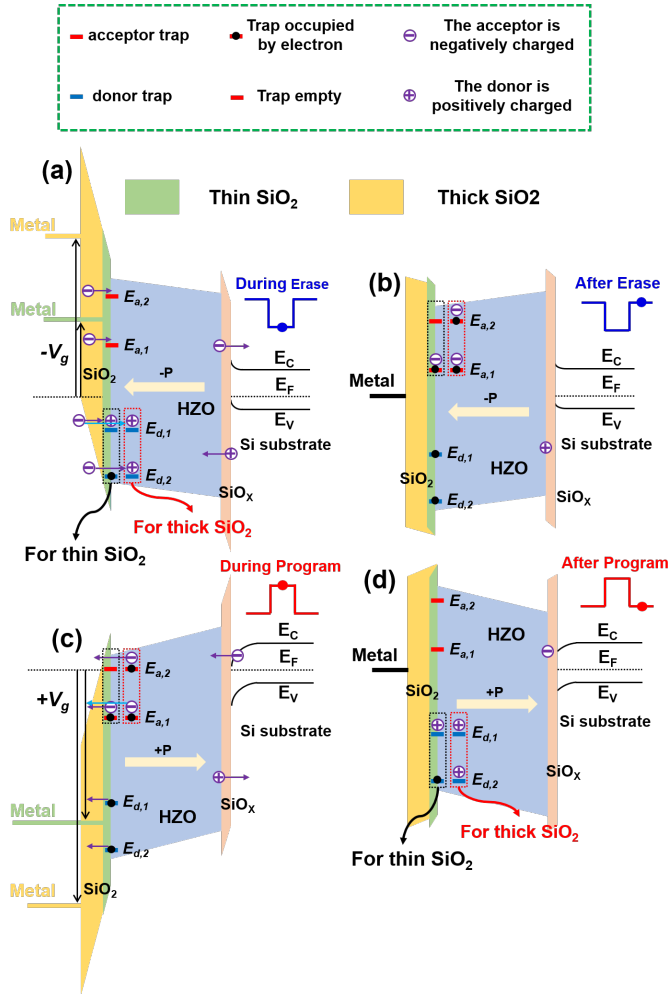


Fig. 8. Band diagram of the MIFIS with different top SiO₂ interlayer thickness: (a) during erase, (b) after erase, (c) during program and (d) after erase.

of the $V_{th,ERS}$ vs. the top SiO₂ thickness curve as shown in Fig. 7(b).

Similarly, we discuss the physical origin of the first stage of the program case. Fig. 8(c) shows the band diagram of the MIFIS during the program operation. During the program operation, the acceptor traps are empty through electrons detrapping and/or holes trapping regardless of the top SiO₂ thickness and show neutral charges. For the SiO₂ thickness of less than 1.7 nm, the Fermi energy level of the gate metal TiN is always located below the donor trap energy level $E_{d,1}$ during the program operation. The donor trap energy level $E_{d,1}$ is also empty and shows positive charges. After the program operation, these positive charges are left as shown in Fig. 8(d) and lead to the positive shift of V_{th} after the program ($V_{th,PGM}$) as shown in Fig. 7(b). Moreover, for the SiO₂ thickness of less than 1.7 nm, these positive charges determined by donor trap energy level $E_{d,1}$ after the program operation are nearly identical and this results in the first stage of the $V_{th,PGM}$ vs. the top SiO₂ thickness curve as shown in Fig. 7(b).

We discuss the physical origin of the second stage of the program case. For the SiO₂ thickness of less than 1.7 nm, the donor trap energy level $E_{d,1}$ is empty and the donor trap energy level $E_{d,2}$ is filled by the electrons. For thicker SiO₂ thickness of larger than 1.7 nm, however, both the donor trap energy levels

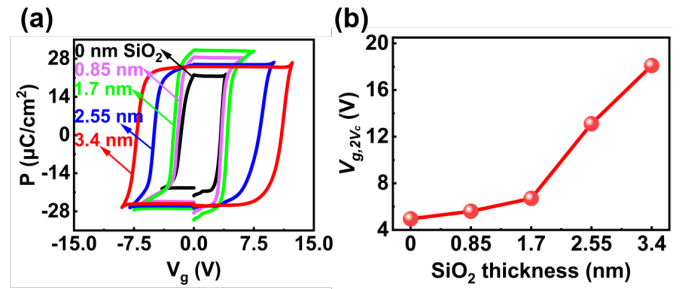


Fig. 9. (a) The results of the PUND measurements. (b) The dependence of $V_{g,2Vc}$ on the top SiO₂ interlayer thickness.

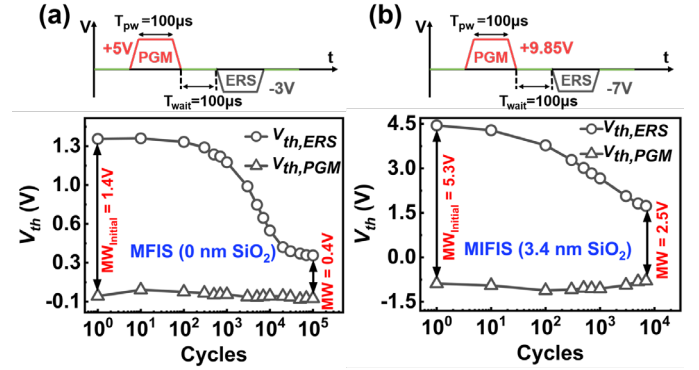


Fig. 10. Endurance characteristics of (a) the MFIS structure and (b) the MIFIS structure with 3.4 nm top SiO₂.

$E_{d,2}$ and $E_{d,1}$ are empty because thicker SiO₂ induces a larger voltage drop across the whole top SiO₂ interlayer and a lower Fermi level of the metal gate with respect to the trap levels as shown in Fig. 8(c). Then more positive charges are left for thicker SiO₂ thickness of larger than 1.7 nm, and result in the second stage of the $V_{th,PGM}$ vs. the top SiO₂ thickness curve as shown in Fig. 7(b). Finally, the above results lead to a two-stage linear dependence between the maximum MW and the top SiO₂ thickness as shown in Fig. 7(a).

The above discussions are verified by the PUND measurement. Fig. 9(a) shows the PUND measurement results. The bulk, source, and drain terminals were shorted during the measurement. As shown in Fig. 9(a), the spontaneous polarization vs. gate voltage (P - V_g) curve broadens with increasing top SiO₂ interlayer thickness. Our measurement results are consistent with [35]. The physical origin of the broadener of the P - V_g curve is attributed to the partial voltage across the top SiO₂ interlayer caused by the trapped charges at the top SiO₂/Hf_{0.5}Zr_{0.5}O₂ interface. We define the distance between the intersections of the P - V_g curve and the V_g axis as $V_{g,2Vc}$. Fig. 9(b) exhibits the dependence of $V_{g,2Vc}$ on the top SiO₂ interlayer thickness. The dependence, which is similar to that of the maximum MW on the top SiO₂ thickness, as shown in Fig. 9(b) further validates the existence of the different interfacial charges Q_{tp} trapped at the top SiO₂/Hf_{0.5}Zr_{0.5}O₂ interface.

C. The endurance and retention characterizations

We study the endurance characteristics of the MIFIS structure. Fig. 10(a) and (b) show the endurance characteristics of the MFIS structure and MIFIS structures, respectively. The MIFIS sample shows an endurance of $\sim 10^4$ cycles when the initial MW is 5.3 V. Additionally, it can be observed that the

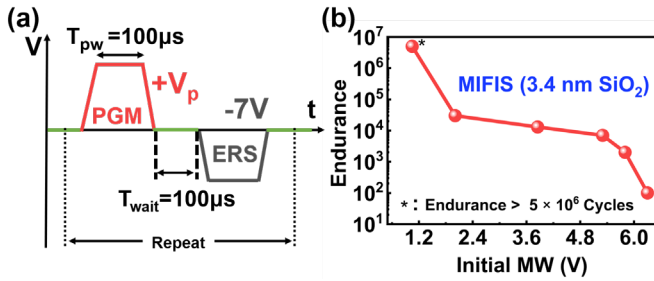


Fig. 11. (a) Waveform of endurance characterization measurement. (b) The dependence of the endurance characteristics on initial MW for MIFIS structure with 3.4 nm top SiO₂.

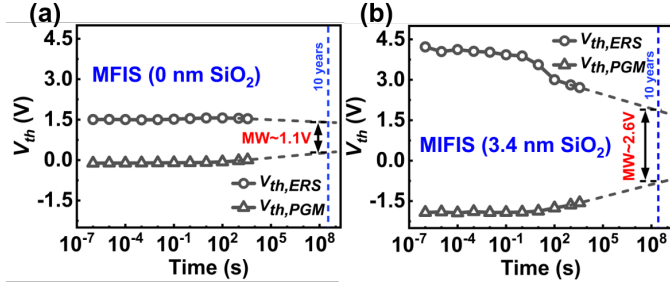


Fig. 12. Retention characteristics measured at room temperature of (a) the MFIS structure and (b) the MIFIS structure with 3.4 nm top SiO₂.

TABLE I
Comparisons of recent research with our work

Structure	Top IL	MW	Endurance	Retention	
Lee et al. from SK Hynix [21] (2022)	MIFIS	SiO ₂	3.8 V	unknow	10 years
Das et al. from GIT [24] (2023)	MFIFIS	Al ₂ O ₃	7.1 V	unknow	10 years
Suzuki et al. from Kioxia [23] (2023)	MIFIS	unknow	2.3 V	~10 ⁶ cycles	10 years
Lim et al. from Samsung [22] (2023)	MIFIS	unknow	3.1 V	~10 ⁶ cycles	10 years
Yoon et al. from SK Hynix [20] (2023)	MIFIS	unknow	5.04 V	~3×10 ³ cycles	10 years
Hu et al. from IMECAS [25] (2024)	MIFIS	Al ₂ O ₃	4.1 V	~1×10 ⁴ cycles	10 years
This work	MIFIS	SiO ₂	5.3 V	~1×10 ⁴ cycles	10 years

window stability of the MIFIS structure is superior to that of the MFIS structure. To evaluate the endurance characteristics of the MIFIS structure more reasonably, we investigate the dependence of the endurance characteristics on the initial MW. Fig. 11(a) shows the waveform of endurance characterization measurement. We change the initial MW by iterating through the amplitudes of the program pulse (8-10.5 V). Fig. 11(b) shows the measurement results. The endurance characteristic degrades with a larger initial MW. This is because a larger

initial MW means more charges tapping and de-trapping, which accelerates the degradation of the interlayer and leads to poorer endurance characteristics.

We study the retention characteristics. Fig. 12 shows the retention characteristics for the two structures under the pulse amplitude of the maximum MW. Both devices have a retention lifetime beyond 10 years.

Table I shows the benchmark of our work. Our work exhibits a larger MW (5.3 V), a better endurance (~1×10⁴ cycles), and a retention lifetime beyond 10 years.

IV. CONCLUSIONS

We study the impact of the top SiO₂ thickness on the MW. We find that the MW increases with a thicker top SiO₂ interlayer. Such an increase exhibits a two-stage linear dependence. We attribute this phenomenon to the presence of different interfacial charges Q_{ip} trapped at the top SiO₂/Hf_{0.5}Zr_{0.5}O₂ interface. Furthermore, we also investigate the dependence of the endurance on initial MW, and find that the endurance characteristic degrades with increasing the initial MW. By inserting a 3.4 nm top SiO₂ interlayer between the gate metal TiN and the ferroelectric Hf_{0.5}Zr_{0.5}O₂, we achieve the maximum MW of 6.3 V. And our device achieves the endurance ~1×10⁴ cycles when the initial MW is ~5.3 V and retention lifetime over 10 years.

REFERENCES

- [1] J. Müller, T. S. Böske, D. Bräuhaus, U. Schröder, U. Böttger, J. Sundqvist, P. Kücher, T. Mikolajick, and L. Frey, "Ferroelectric Zr_{0.5}Hf_{0.5}O₂ thin films for nonvolatile memory applications," *Appl. Phys. Lett.*, vol. 99, no. 11, Sept. 2011, doi: 10.1063/1.3636417.
- [2] M. Trentzsch, S. Flachowsky, R. Richter, J. Paul, B. Reimer, D. Utes, S. Jansen, H. Mulaosmanovic, S. Müller, S. Slesazek, J. Ocker, M. Noack, J. Müller, P. Polakowski, J. Schreiter, S. Beyer, T. Mikolajick, and B. Rice, "A 28nm HKMG super low power embedded NVM technology based on ferroelectric FETs," in *IEDM Tech. Dig.*, Dec. 2016, pp. 11.5.1-11.5.4, doi: 10.1109/IEDM.2016.7838397.
- [3] Z. Cai, K. Toprasertpong, M. Takenaka, and S. Takagi, "HZO Scaling and Fatigue Recovery in FeFET with Low Voltage Operation: Evidence of Transition from Interface Degradation to Ferroelectric Fatigue," in *Proc. Symp. VLSI Technol.*, Jun. 2023, pp. 1-2, doi: 10.23919/VLSITechnologyandCir57934.2023.10185295.
- [4] Y. Peng, W. Xiao, F. Liu, C. Jin, Y. Cheng, L. Wang, Y. Zhang, X. Yu, Y. Liu, Y. Hao, and G. Han, "HfO₂-ZrO₂ Superlattice Ferroelectric Field-Effect Transistor With Improved Endurance and Fatigue Recovery Performance," *IEEE Trans. Electron Devices*, vol. 70, no. 7, pp. 3979-3982, Jul. 2023, doi: 10.1109/TED.2023.3279063.
- [5] H. Mulaosmanovic, E. T. Breyer, T. Mikolajick, and S. Slesazek, "Recovery of Cycling Endurance Failure in Ferroelectric FETs by Self-Heating," *IEEE Electron Device Lett.*, vol. 40, no. 2, pp. 216-219, Feb. 2019, doi: 10.1109/LED.2018.2889412.
- [6] K. Ni, P. Sharma, J. Zhang, M. Jerry, J. A. Smith, K. Tapily, R. Clark, S. Mahapatra, and S. Datta, "Critical Role of Interlayer in Hf_{0.5}Zr_{0.5}O₂ Ferroelectric FET Nonvolatile Memory Performance," *IEEE Trans. Electron Devices*, vol. 65, no. 6, pp. 2461-2469, Jun. 2018, doi: 10.1109/ted.2018.2829122.
- [7] A. J. Tan, M. Pešić, L. Larcher, Y. H. Liao, L. C. Wang, J. H. Bae, C. Hu, and S. Salahuddin, "Hot Electrons as the Dominant Source of Degradation for Sub-5nm HZO FeFETs," in *Proc. Symp. VLSI Technol.*, Jun. 2020, pp. 1-2, doi: 10.1109/VLSITechnology18217.2020.9265067.
- [8] S. W. Kim, W. Shin, M. Kim, K. R. Kwon, J. Yim, J. Kim, C. Han, S. Jeong, E. C. Park, J. W. You, H. Kim, R. Choi, and D. Kwon, "Ferroelectric Field-Effect Transistor Synaptic Device With Hafnium-Silicate Interlayer," *IEEE Electron Device Lett.*, vol. 44, no. 12, pp. 1955-1958, Dec. 2023, doi: 10.1109/LED.2023.3324695.

- [9] E. J. Shin, S. W. Shin, S. H. Lee, T. I. Lee, M. J. Kim, H. J. Ahn, J. H. Kim, W. S. Hwang, J. Lee, and B. J. Cho, "Capacitance Boosting by Anti-Ferroelectric Blocking Layer in Charge Trap Flash Memory Device," in *IEDM Tech. Dig.*, Dec. 2020, pp. 6.2.1-6.2.4, doi: 10.1109/IEDM13553.2020.9371984.
- [10] K. T. Chen, H. Y. Chen, C. Y. Liao, G. Y. Siang, C. Lo, M. H. Liao, K. S. Li, S. T. Chang, and M. H. Lee, "Non-Volatile Ferroelectric FETs Using 5-nm Hf_{0.5}Zr_{0.5}O₂ With High Data Retention and Read Endurance for 1T Memory Applications," *IEEE Electron Device Lett.*, vol. 40, no. 3, pp. 399-402, Mar. 2019, doi: 10.1109/LED.2019.2896231.
- [11] J. Chai, H. Xu, J. Xiang, Y. Zhang, L. Zhou, S. Zhao, F. Tian, J. Duan, K. Han, X. Wang, J. Luo, W. Wang, T. Ye, and Y. Guo, "First-principles study of oxygen vacancy defects in orthorhombic Hf_{0.5}Zr_{0.5}O₂/SiO₂/Si gate stack," *J. Appl. Phys.*, vol. 132, no. 10, Sept. 2022, doi: 10.1063/5.0106750.
- [12] Q. H. Shao, G. X. Liu, D. Teweldebrhan, A. A. Balandin, S. Runyantsev, M. S. Shur, and D. Yan, "Flicker Noise in Bilayer Graphene Transistors," *IEEE Electron Device Lett.*, vol. 30, no. 3, pp. 288-290, Mar. 2009, doi: 10.1109/LED.2008.2011929.
- [13] M. Si, X. Lyu, and P. D. Ye, "Ferroelectric Polarization Switching of Hafnium Zirconium Oxide in a Ferroelectric/Dielectric Stack," *ACS Appl. Electron. Mater.*, vol. 1, no. 5, pp. 745-751, May 2019, doi: 10.1021/acsaelm.9b00092.
- [14] T. S. Böscke, J. Müller, D. Bräuhaus, U. Schröder, and U. Böttger, "Ferroelectricity in hafnium oxide thin films," *Appl. Phys. Lett.*, vol. 99, no. 10, Sept. 2011, doi: 10.1063/1.3634052.
- [15] N. Gong, and T. P. Ma, "A Study of Endurance Issues in HfO₂-Based Ferroelectric Field Effect Transistors: Charge Trapping and Trap Generation," *IEEE Electron Device Lett.*, vol. 39, no. 1, pp. 15-18, Jan. 2018, doi: 10.1109/LED.2017.2776263.
- [16] K. Toprasertpong, Z. Y. Lin, T. E. Lee, M. Takenaka, and S. Takagi, "Asymmetric Polarization Response of Electrons and Holes in Si FeFETs: Demonstration of Absolute Polarization Hysteresis Loop and Inversion Hole Density over $2 \times 10^{13} \text{ cm}^{-2}$," in *Proc. Symp. VLSI Technol.*, Jun. 2020, pp. 1-2, doi: 10.1109/VLSITechnology18217.2020.9265015.
- [17] E. Yurchuk, J. Müller, S. Müller, J. Paul, M. Pešić, R. v. Bentum, U. Schroeder, and T. Mikolajick, "Charge-Trapping Phenomena in HfO₂-Based FeFET-Type Nonvolatile Memories," *IEEE Trans. Electron Devices*, vol. 63, no. 9, pp. 3501-3507, Sept. 2016, doi: 10.1109/TED.2016.2588439.
- [18] B. Zeng, M. Liao, J. Liao, W. Xiao, Q. Peng, S. Zheng, and Y. Zhou, "Program/Erase Cycling Degradation Mechanism of HfO₂-Based FeFET Memory Devices," *IEEE Electron Device Lett.*, vol. 40, no. 5, pp. 710-713, May. 2019, doi: 10.1109/LED.2019.2908084.
- [19] C. Y. Chan, K. Y. Chen, H. K. Peng, and Y. H. Wu, "FeFET Memory Featuring Large Memory Window and Robust Endurance of Long-Pulse Cycling by Interface Engineering using High-k AlON," in *Proc. Symp. VLSI Technol.*, Jun. 2020, pp. 1-2, doi: 10.1109/VLSITechnology18217.2020.9265103.
- [20] H.-K. Peng, C.-Y. Chan, K.-Y. Chen, and Y.-H. Wu, "Enabling large memory window and high reliability for FeFET memory by integrating AlON interfacial layer," *Appl. Phys. Lett.*, vol. 118, no. 10, pp. 103503, Mar. 2021, doi: 10.1063/5.0036824.
- [21] A. J. Tan, Y. H. Liao, L. C. Wang, N. Shanker, J. H. Bae, C. Hu, and S. Salahuddin, "Ferroelectric HfO₂ Memory Transistors With High-κ Interfacial Layer and Write Endurance Exceeding 10¹⁰ Cycles," *IEEE Electron Device Lett.*, vol. 42, no. 7, pp. 994-997, July. 2021, doi: 10.1109/LED.2021.3083219.
- [22] A. J. Tan, A. K. Yadav, K. Chatterjee, D. Kwon, S. Kim, C. Hu, and S. Salahuddin, "A Nitrided Interfacial Oxide for Interface State Improvement in Hafnium Zirconium Oxide-Based Ferroelectric Transistor Technology," *IEEE Electron Device Lett.*, vol. 39, no. 1, pp. 95-98, Jan. 2018, doi: 10.1109/LED.2017.2772791.
- [23] S. Dai, S. Li, S. Xu, F. Tian, J. Chai, J. Duan, W. Xiong, J. Xiang, Y. Wang, H. Xu, J. Zhang, X. Wang, and W. Wang, "Role of Nitrogen in Suppressing Interfacial States Generation and Improving Endurance in Ferroelectric Field Effect Transistors," in *Proc. IEEE Int. Memory Workshop (IMW)*, May. 2024, pp. 1-4, doi: 10.1109/IMW59701.2024.10536971.
- [24] S. Deng, Z. Liu, X. Li, T. P. Ma, and K. Ni, "Guidelines for Ferroelectric FET Reliability Optimization: Charge Matching," *IEEE Electron Device Lett.*, vol. 41, no. 9, pp. 1348-1351, Sept. 2020, doi: 10.1109/LED.2020.3011037.
- [25] T. Kim, J. Hwang, G. Kim, M. Jung, and S. Jeon, "High-Performance and High-Endurance HfO₂-Based Ferroelectric Field-Effect Transistor Memory with a Spherical Recess Channel," *Physica status solidi (RRL) – Rapid Research Letters*, vol. 15, no. 5, pp. 2100018, May 2021, doi: 10.1002/pssr.202100018.
- [26] M. Liao, H. Xu, J. Duan, S. Zhao, F. Tian, J. Chai, K. Han, Y. Jiang, J. Xiang, W. Wang, and X. Wang, "Impact of Saturated Spontaneous Polarization on the Endurance Fatigue of Si FeFET With Metal/Ferroelectric/Interlayer/Si Gate Structure," *IEEE Trans. Electron Devices*, vol. 70, no. 8, pp. 4055-4061, Aug. 2023, doi: 10.1109/TED.2023.3285715.
- [27] F. Tian, S. Zhao, H. Xu, J. Xiang, T. Li, W. Xiong, J. Duan, J. Chai, K. Han, X. Wang, W. Wang, and T. Ye, "Impact of Interlayer and Ferroelectric Materials on Charge Trapping During Endurance Fatigue of FeFET With TiN/Hf_xZr_{1-x}O₂/Interlayer/Si (MIFIS) Gate Structure," *IEEE Trans. Electron Devices*, vol. 68, no. 11, pp. 5872-5878, Nov. 2021, doi: 10.1109/TED.2021.3114663.
- [28] Z. Chen, N. Ronchi, A. Walke, K. Banerjee, M. I. Popovici, K. Katcko, G. V. D. Bosch, M. Rosmeulen, V. Afanas'Ev, and J. V. Houdt, "Improved MW of IGZO-channel FeFET by Reading Scheme Optimization and Interfacial Engineering," in *Proc. IEEE Int. Memory Workshop (IMW)*, May 2023, pp. 1-4, doi: 10.1109/IMW56887.2023.10145930.
- [29] T. Cui, D. Chen, Y. Dong, Y. Fan, Z. Yao, H. Duan, J. Liu, G. Liu, M. Si, and X. Li, "Can Interface Layer be Really Free for Hf_xZr_{1-x}O₂ Based Ferroelectric Field-Effect Transistors With Oxide Semiconductor Channel?," *IEEE Electron Device Lett.*, vol. 45, no. 3, pp. 368-371, Mar. 2024, doi: 10.1109/LED.2024.3355523.
- [30] Q. Li, S. Wang, Z. Li, X. Hu, Y. Liu, J. Yu, Y. Yang, T. Wang, J. Meng, Q. Sun, D. W. Zhang, and L. Chen, "High-performance ferroelectric field-effect transistors with ultra-thin indium tin oxide channels for flexible and transparent electronics," *Nat. Commun.*, vol. 15, no. 1, pp. 2686, Mar. 2024, doi: 10.1038/s41467-024-46878-5.
- [31] P. D. Lomenzo, Q. Takmeel, C. M. Fancher, C. Zhou, N. G. Rudawski, S. Moghaddam, J. L. Jones, and T. Nishida, "Ferroelectric Si-Doped HfO₂ Device Properties on Highly Doped Germanium," *IEEE Electron Device Lett.*, vol. 36, no. 8, pp. 766-768, Aug. 2015, doi: 10.1109/LED.2015.2445352.
- [32] F. Mo, Y. Tagawa, C. Jin, M. Ahn, T. Saraya, T. Hiramoto, and M. Kobayashi, "Experimental Demonstration of Ferroelectric HfO₂ FET with Ultrathin-body IGZO for High-Density and Low-Power Memory Application," in *Proc. Symp. VLSI Technol.*, Jun. 2019, pp. T42-T43, doi: 10.23919/VLSIT.2019.8776553.
- [33] S. Yoon, S. I. Hong, D. Kim, G. Choi, Y. M. Kim, K. Min, S. Kim, M. H. Na, and S. Cha, "QLC Programmable 3D Ferroelectric NAND Flash Memory by Memory Window Expansion using Cell Stack Engineering," in *Proc. Symp. VLSI Technol.*, Jun. 2023, pp. 1-2, doi: 10.23919/VLSITechnologyandCir57934.2023.10185294.
- [34] J.-G. Lee, J. Kim, D. I. Suh, I. Kim, G. D. Han, S. W. Ryu, S. Lee, M.-H. Na, S. Y. Cha, H. W. Park, and C. S. Hwang, "Memory Window Expansion for Ferroelectric FET based Multilevel NVM: Hybrid Solution with Combination of Polarization and Injected Charges," in *Proc. IEEE Int. Memory Workshop (IMW)*, May 2022, pp. 1-4, doi: 10.1109/imw52921.2022.9779292.
- [35] S. Lim, T. Kim, I. Myeong, S. Park, S. Noh, S. M. Lee, J. Woo, H. Ko, Y. Noh, M. Choi, K. Lee, S. Han, J. Baek, K. Kim, J. Kim, D. Jung, K. Kim, S. Yoo, H. J. Lee, S. G. Nam, J. S. Kim, J. Park, C. Kim, S. Kim, H. Kim, J. Heo, K. Park, S. Jeon, W. Kim, D. Ha, Y. G. Shin, and J. Song, "Comprehensive Design Guidelines of Gate Stack for QLC and Highly Reliable Ferroelectric VNAND," in *IEDM Tech. Dig.*, Dec. 2023, pp. 1-4, doi: 10.1109/IEDM45741.2023.10413820.
- [36] K. Suzuki, K. Sakuma, Y. Yoshimura, R. Ichihara, K. Matsuo, D. Hagishima, M. Fujiwara, and M. Saitoh, "High-Endurance FeFET with Metal-Doped Interfacial Layer for Controlled Charge Trapping and Stabilized Polarization," in *IEDM Tech. Dig.*, Dec. 2023, pp. 1-4, doi: 10.1109/IEDM45741.2023.10413699.
- [37] D. Das, H. Park, Z. Wang, C. Zhang, P. V. Ravindran, C. Park, N. Afroz, P. K. Hsu, M. Tian, H. Chen, W. Chern, S. Lim, K. Kim, K. Kim, W. Kim, D. Ha, S. Yu, S. Datta, and A. Khan, "Experimental demonstration and modeling of a ferroelectric gate stack with a tunnel dielectric insert for NAND applications," in *IEDM Tech. Dig.*, Dec. 2023, pp. 1-4, doi: 10.1109/IEDM45741.2023.10413697.
- [38] T. Hu, X. Sun, M. Bai, X. Jia, S. Dai, T. Li, R. Han, Y. Ding, H. Fan, Y. Zhao, J. Chai, H. Xu, M. Si, X. Wang, and W. Wang, "Enlargement of Memory Window of Si Channel FeFET by Inserting Al₂O₃ Interlayer on Ferroelectric Hf_{0.5}Zr_{0.5}O₂," *IEEE Electron Device Lett.*, pp. 825-828, May 2024, doi: 10.1109/LED.2024.3381966.